Eur. Phys. J. Plus (2014) **129**: 249
DOI 10.1140/epjp/i2014-14249-1

THE EUROPEAN PHYSICAL JOURNAL PLUS

Regular Article

Nanoparticles analysis on the blood flow through a tapered catheterized elastic artery with overlapping stenosis

S. Nadeem[a] and S. Ijaz

Department of Mathematics, Quaid-i-Azam University 45320, Islamabad 44000, Pakistan

Received: 16 September 2014
Published online: 18 November 2014 –

Abstract. This paper is concerned with the analysis of blood through an annulus, bounded between an arterial stenosis and a uniform catheter. The nature of blood through coaxial tubes is considered as that of a nano viscous fluid. The mild stenosis approximation and corresponding boundary conditions are used to obtain analytic expressions for axial velocity, temperature distribution, nanoparticle volume fraction, wall shear stress and resistance impedance to flow. The model is also used to study the consequence of thermophoresis, Brownian motion, local nanoparticle Grashof and local temperature Grashof numbers on the flow by plotting graphs and streamlines. The variation with different flow parameters through tables is also discussed to understand the effects of stenosis height in constricted annular regions.

1 Introduction

The study of the physiology and anatomy of a biological system depends on the knowledge of the blood flow through arteries. The progress and cause of various arterial diseases are related to the mechanical behavior and the flow characteristics of blood vessel walls. The unnatural and abnormal growth in the arterial wall thickness at different locations of the cardiovascular system is medically termed as stenosis. Its occurrence in one or more locations confines the blood flow through the lumen of the coronary arteries. Once the reduction has matured, it brings about significant changes in the blood flow, *i.e.* wall shear stress, resistance impedance to the flow and pressure distribution. The fact that hemodynamic features play a creditable role in the growth of the disease has attracted many researchers to explore modern mathematical models for the flow through tapered arteries by considering blood as either a viscous or non-viscous fluid [1–6].

A small number of studies have been carried out on multiple stenosis. Mekheimer *et al.* [7] discussed the mathematical model for blood flow through an elastic artery with overlapping stenosis. They explored the effect of an induced magnetic field on the blood flow through stenosis by treating blood as a viscous fluid. Chakravarty *et al.* [8] discussed the problem of the blood flow through a confined vessel segment with an overlapping stenosis. They explored the two-dimensional non-linear mathematical model of blood flow in tapered arteries in the presence of stenosis. Mekheimer *et al.* [9] discussed the effects of heat and chemical reactions on the blood flow through anisotropically tapered elastic artery with overlapping stenosis. They explored the nature of blood in small arteries mathematically by treating it as a micropolar fluid. Ismail *et al.* [10] discussed the power-law model of the blood flow through an overlapping stenosed artery where they explored the vascular wall by considering it as an elastic wall. For more details, see refs. [11–13].

The inclusion of a catheter into an artery produces an annular region between the arterial wall and the catheter wall. A catheter is composed of polyester-based thermoplastic polyurethane, chlorides and medical grade polyvinyl, etc. The insertion of a catheter into arteries will change the flow field and modify the hemodynamics conditions that occur in the artery before catheterization [14,15]. Mekheimer *et al.* [16] carried out a study that is related with the surgical technique for the injection of the catheter through stenotic arteries. They explored the movement of the physiological fluid on behalf of blood in the gap between two eccentric tubes. Srivastava *et al.* [17] discussed the blood flow in a narrow catheterized artery. They investigated it by using a two-phase macroscopic model of blood. Verma *et al.* [18] discussed the problem of the blood flow through a symmetric stenosis during artery catheterization by assuming blood to behave like a viscous fluid.

Nanofluid is a mixture of nanosize particles suspended in the base fluid which has a greater thermal conductivity as compared to the base fluid. Due to their potential in the enhancement of heat transfer, nanofluids have attracted enormous interest for researchers, such that many have investigated different features of nanofluids. Nanofluids were

[a] e-mail: snqau@hotmail.com

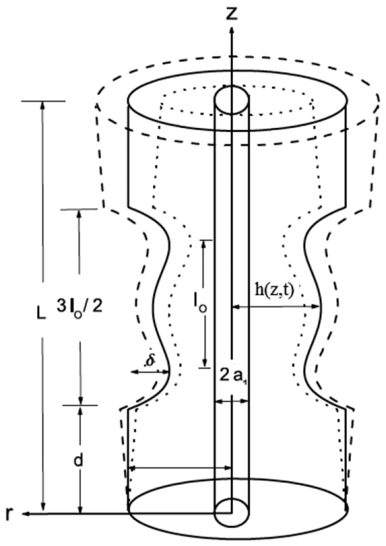

Fig. 1. Geometry of the overlapping stenosed artery.

firstly discussed by Choi [19], who explored the suspension of nanoparticles into base fluids with the typical length scale of 1–100 nm. Later on, other researchers discussed different mathematical nanomodels, *e.g.*, [20–24]. Nadeem *et al.* [25,26] discussed the nanoparticles analysis of the blood flow through tapered arteries. They stated that the hemodynamics effects play an important role due to the formation of the stenosis. Akbar *et al.* [27] performed a theoretical analysis of nanoparticles through the composite stenosed arteries. They explored the viscous nanofluid flow model through tapered arteries with permeable walls along the slip on stenosis. Ellahi *et al.* [28] discussed the mathematical models of a Jeffrey fluid with nanoparticles in the tapered stenosed atherosclerotic arteries. They explored convection effects of heat transfer with catheter under mild stenosis. Recently, Nadeem *et al.* [29] discussed the influence of the induced magnetic field on the blood flow with stenosis. They explored the effects of nanoparticles with heat and mass transfer on wall shear stress and resistance impedance to the flow.

Inspired by the above studies, the article reported here is devoted to the study of the nano viscous model of the blood flow through overlapping stenosed arteries with a catheter. The non-dimensional governing equations in the case of mild stenosis and the corresponding boundary conditions are arranged and then solved by using the homotopy perturbation method (HPM) [30,31]. The solutions contains thermophoresis number N_t, Brownian motion number N_b, local nanoparticle Grashof number G_r and local temperature Grashof number B_r. At the end, the effects of these flow parameters are explored for wall shear stress, resistance impedance to the flow, temperature distribution, nanoparticle volume fraction and axial velocity.

2 Formulation of the problem

We consider the steady, laminar and the incompressible viscous nanofluid flowing through a tube of length L and a catheter of radius a_1 with overlapping stenosis. Let (r, θ, z) be defined as coordinates in the cylindrical polar coordinate system, where the z-axis is taken along the axis of the artery, while θ and r are taken along the circumferential and radial directions, respectively. The heat transfer phenomenon is taken into account by giving temperature T_0 and concentration C_0 to the upper wall of the catheter. The geometry of the elastic arterial wall of the time-variant overlapping stenosis for different taper angles is defined as [7]

$$\begin{aligned}\bar{h}(z,t) &= \left[(m^*z + e_0) - \frac{\delta^* \cos\phi}{L_0}(\bar{z} - d^*)\left\{11 - \frac{94}{3L_0}(\bar{z} - d^*) + \frac{32}{L_0^2}(\bar{z} - d^*)^2 - \frac{32}{3L_0^3}(\bar{z} - d^*)^3\right\}\right] Q_1(t),\\ &= (m^*\bar{z} + e_0)Q_1(t), \qquad \text{otherwise} \qquad d^* \le \bar{z} \le d^* + \frac{3}{2L_0}, \end{aligned} \tag{1}$$

where $h(z,t)$ is the radius of the tapered arterial segment in the trapped region, e_0 the constant radius in the non-stenotic region, ϕ the tapered angle, $\frac{3}{2L_0}$ the length of overlapping stenosis, d the location of the stenosis, $\delta \cos\phi$ is taken to be the critical height of the overlapping stenosis and $m = \tan\phi$ represents the slope of the tapered vessel. We can explore the possibility of different shapes of the artery, the converging tapering ($\phi < 0$), non-tapered artery ($\phi = 0$) and the diverging tapering ($\phi > 0$). The time-variant parameter is taken to be

$$Q_1(t) = 1 - \alpha(\cos wt - 1)\exp[-\alpha wt], \tag{2}$$

where α is a constant, w represents the angular frequency of the forced oscillation and t is the time. (See fig. 1.)

The governing equations for the nano viscous fluid can be written as

$$\frac{\partial \bar{u}}{\partial \bar{r}} + \frac{\bar{u}}{\bar{r}} + \frac{\partial \bar{w}}{\partial \bar{z}} = 0, \tag{3}$$

$$\rho_f \left(\frac{\partial \bar{u}}{\partial \bar{t}} + \bar{u}\frac{\partial \bar{u}}{\partial \bar{r}} + \bar{w}\frac{\partial \bar{u}}{\partial \bar{z}} \right) = -\frac{\partial \bar{p}}{\partial \bar{r}} + \left(\frac{\partial^2 \bar{u}}{\partial \bar{r}^2} + \frac{1}{\bar{r}}\frac{\partial \bar{u}}{\partial \bar{r}} + \frac{\partial^2 \bar{u}}{\partial \bar{z}^2} - \frac{\bar{u}^2}{\bar{r}^2} \right), \tag{4}$$

$$\rho_f \left(\frac{\partial \bar{w}}{\partial \bar{t}} + \bar{u}\frac{\partial \bar{w}}{\partial \bar{r}} + \bar{w}\frac{\partial \bar{w}}{\partial \bar{z}} \right) = -\frac{\partial \bar{p}}{\partial \bar{z}} + \left(\frac{\partial^2 \bar{w}}{\partial \bar{r}^2} + \frac{1}{\bar{r}}\frac{\partial \bar{w}}{\partial \bar{r}} + \frac{\partial^2 \bar{w}}{\partial \bar{z}^2} \right) + \rho_f g \alpha_t (\bar{T} - \bar{T}_1) + \rho_f g \alpha_c (\bar{C} - \bar{C}_1), \tag{5}$$

$$\left(\bar{u}\frac{\partial \bar{T}}{\partial \bar{r}} + \bar{w}\frac{\partial \bar{T}}{\partial \bar{z}} \right) = \alpha \left(\frac{\partial^2 \bar{T}}{\partial \bar{r}^2} + \frac{1}{\bar{r}}\frac{\partial \bar{T}}{\partial \bar{r}} + \frac{\partial^2 \bar{T}}{\partial \bar{z}^2} \right) + \tau \left[D_{\bar{B}} \left(\frac{\partial \bar{C}}{\partial \bar{r}}\frac{\partial \bar{T}}{\partial \bar{r}} + \frac{\partial \bar{C}}{\partial \bar{z}}\frac{\partial \bar{T}}{\partial \bar{z}} \right) + \frac{D_{\bar{T}}}{\bar{T}_1} \left\{ \left(\frac{\partial \bar{T}}{\partial \bar{r}} \right)^2 + \left(\frac{\partial \bar{T}}{\partial \bar{z}} \right)^2 \right\} \right], \tag{6}$$

$$\left(\bar{u}\frac{\partial \bar{C}}{\partial \bar{r}} + \bar{w}\frac{\partial \bar{C}}{\partial \bar{z}} \right) = D_{\bar{B}} \left(\frac{\partial^2 \bar{C}}{\partial \bar{r}^2} + \frac{1}{\bar{r}}\frac{\partial \bar{C}}{\partial \bar{r}} + \frac{\partial^2 \bar{C}}{\partial \bar{z}^2} \right) + \frac{D_{\bar{T}}}{\bar{T}_1} \left(\frac{\partial^2 \bar{T}}{\partial \bar{r}^2} + \frac{1}{\bar{r}}\frac{\partial \bar{T}}{\partial \bar{r}} + \frac{\partial^2 \bar{T}}{\partial \bar{z}^2} \right). \tag{7}$$

For the above equation τ describes the ratio between the material heat capacity of nanoparticles and fluid heat capacity, $D_{\bar{B}}$ the Brownian diffusion coefficient, $D_{\bar{T}}$ the thermophoretic diffusion coefficient, α_t the coefficient of thermal expansion and α_c the coefficient of thermal expansion with nanoconcentration.

Non-dimensional variables are defined as

$$\begin{aligned}
r &= \frac{\bar{r}}{e_0}, \qquad z = \frac{\bar{z}}{L_0}, \qquad w = \frac{\bar{w}}{u_o}, \qquad u = \frac{L_0 \bar{u}}{u_o \delta}, \qquad \bar{p} = \frac{e_0^2 p}{u_o L_0 \mu}, \qquad t = \frac{\bar{t} u_o}{L_0}, \\
R_{en} &= \frac{L_0 u_o \rho}{\mu}, \qquad \theta = \frac{T - \bar{T}_1}{\bar{T}_0 - \bar{T}_1}, \qquad \sigma = \frac{\bar{C} - \bar{C}_1}{\bar{C}_0 - \bar{C}_1}, \qquad N_t = \frac{(\rho c)_p D_{\bar{T}}}{(\rho c)_f \alpha}, \\
\alpha &= \frac{k}{(\rho c)_f}, \qquad N_t = \frac{(\rho c)_p D_B \bar{C}_o}{(\rho c)_f \alpha}, \qquad B_r = \frac{\rho g \alpha_c e_0^2 (\bar{C}_0 - \bar{C}_1)}{\mu u_o}, \\
G_r &= \frac{\rho g \alpha_t e_0^2 (\bar{T}_0 - \bar{T}_1)}{\mu u_o}.
\end{aligned} \tag{8}$$

For the above equations, R_{en} is the Reynolds number, N_b the Brownian motion parameter, B_r the local nanoparticle Grashof number, G_r the local temperature Grashof and N_t the thermophoresis parameter. Using the above eq. (8), the mild stenosis case $\delta^* = \frac{\delta}{e_0} \ll 1$ and the extra condition $\epsilon = \frac{e_0}{b} \backsim O(1)$, the constitutive eqs. (1) to (7) can be written as

$$\frac{\partial p}{\partial r} = 0, \tag{9}$$

$$\frac{\partial p}{\partial z} = \frac{1}{r}\left(\frac{\partial}{\partial r}\left(r\frac{\partial w}{\partial r} \right) \right) + G_r \theta + B_r \sigma, \tag{10}$$

$$\frac{1}{r}\frac{\partial}{\partial r}\left(r\frac{\partial \theta}{\partial r} \right) + N_b \left(\frac{\partial \sigma}{\partial r} \right)\left(\frac{\partial \theta}{\partial r} \right) + N_t \left(\frac{\partial \theta}{\partial r} \right)^2 = 0, \tag{11}$$

$$\left(\frac{1}{r}\frac{\partial}{\partial r}\left(r\frac{\partial \sigma}{\partial r} \right) \right) + \frac{N_t}{N_b}\left(\frac{1}{r}\frac{\partial}{\partial r}\left(r\frac{\partial \theta}{\partial r} \right) \right) = 0, \tag{12}$$

The boundary conditions and the geometry of stenosis in dimensionless form are defined as

$$\begin{aligned}
h(z,t) &= \left[(mz+1) - \delta \cos\phi (z-d) \left\{ 11 - \frac{94}{3}(z-d) + 32(z-d)^2 - \frac{32}{3}(z-d)^3 \right\} \right] Q_1(t), \\
&= (mz+1)Q_1(t), \qquad \text{otherwise} \qquad d \le z \le d + \frac{3}{2},
\end{aligned} \tag{13}$$

$$w = 0 \quad \text{at} \quad r = h(z), \quad w = 0 \quad \text{at} \quad r = R_c, \tag{14}$$

$$\theta = 0 \quad \text{at} \quad r = h(z), \quad \theta = 1 \quad \text{at} \quad r = R_c, \tag{15}$$

$$\sigma = 0 \quad \text{at} \quad r = h(z), \quad \sigma = 1 \quad \text{at} \quad r = R_c, \tag{16}$$

where, in the above,

$$\delta = \frac{\delta^*}{e_0}, \qquad \sigma = \frac{d}{L_0}, \qquad m^* = \frac{mL_0}{e_0}. \tag{17}$$

For the solution of eqs. (11) and (12), the HPM suggests that we can write these equation as follows [29,30]:

$$H(\Sigma,\theta) = (1-\Sigma)[\Gamma(\theta) - \Gamma(\theta_{10})] + \Sigma\left[\Gamma(\theta) + N_b\left(\frac{\partial\theta}{\partial r}\right)\left(\frac{\partial\sigma}{\partial r}\right) + N_t\left(\frac{\partial\theta}{\partial r}\right)^2\right], \tag{18}$$

$$H(\Sigma,\sigma) = (1-\Sigma)\left[\Gamma(\sigma) - \Gamma(\sigma_{10})\right] + \Sigma\left[\Gamma(\sigma) + \frac{N_t}{N_b}\left(\frac{1}{r}\frac{\partial}{\partial r}\left(r\frac{\partial\theta}{\partial r}\right)\right)\right]. \tag{19}$$

The linear operator and the initial guesses are chosen and defined as

$$\Gamma_r\theta = \frac{1}{r}\frac{\partial}{\partial r}\left(r\frac{\partial}{\partial r}\right), \qquad \Gamma_r\sigma = \frac{1}{r}\frac{\partial}{\partial r}\left(r\frac{\partial}{\partial r}\right), \tag{20}$$

$$\theta_{10}(r,z) = -\left(\frac{r-h}{h-R_c}\right), \qquad \sigma_{10}(r,z) = -\left(\frac{r-h}{h-R_c}\right). \tag{21}$$

According to the HPM, we may define

$$\begin{aligned}\theta &= \theta_0 + \Sigma\theta_1 + O(\Sigma)^2,\\ \sigma &= \sigma_0 + \Sigma\sigma_1 + O(\Sigma)^2.\end{aligned} \tag{22}$$

Making use of eq. (22) into eqs. (18) and (19) for $\Sigma \to 1$, the temperature profile and the nanoparticle volume fraction are written as

$$\begin{aligned}\theta = &-\frac{r-h}{h-R_c} + \frac{1}{4(\ln h - \ln R_c)(h-R_c)^2}\Big(4h(r\ln h - h\ln r + (h-r)\\ &\ln R_c) - \Big(r^2(\ln h - \ln R_c) + h^2(-\ln r + \ln R_c)\Big)(N_b+N_t) - 4\Big((h+r)\\ &\ln h - 2h\ln r + (h-r)\ln R_c\Big)R_c + (\ln h - \ln r)(4+N_b+N_t)R_c^2\Big),\end{aligned} \tag{23}$$

$$\sigma = \frac{(N_b+N_t)(r\ln h - h\ln r + (h-r)\ln R_c + (-\ln h + \ln r)R_c}{(\ln h - \ln R_c)N_b(h-R_c)}. \tag{24}$$

Using eqs. (23) and (24), we can find the exact solution for the axial velocity of eq. (10),

$$\begin{aligned}w = &\frac{\mathrm{d}p}{\mathrm{d}z}\frac{r^2(\ln h - \ln R_c) + h^2(-\ln r + \ln R_c) + R_c^2(-\ln h + \ln r)}{4(\ln h - \ln R_c)}\\ &+ \frac{1}{144(\ln h - \ln R_c)}\Big(\Big(-h^2(36a_1 - 27a_4 + h(16a_2 + 9a_3h)) + 9(4a_1 - 3a_4)r^2\\ &+ 16a_2r^3 + 9a_3r^4\Big)\ln R_c + \ln r\Big(h^2\Big(36a_1 - 27a_4 + h(16a_2 + 9ha_3)\Big)\\ &+ 36a_4r^2\ln R_c\Big) - \ln h\Big(r^2(36a_1 - 27a_4 + r(16a2 + 9a_3r)\Big) + 36\\ &a_4\Big((-h^2+r^2)\ln r + h^2\ln R_c\Big)\Big) + (\ln h - \ln r)R_c^2\Big(9(4a_1 - 3a_4 + 4a_4\ln R_c)\\ &+ 16a_2R_c + 9a_3R_c^2\Big)\Big).\end{aligned} \tag{25}$$

The flow rate is given as

$$F = \int_{R_c}^{h} rw\mathrm{d}r. \tag{26}$$

Using eq. (26) into eq. (25), we get the expression for the pressure gradient as follows:

$$\frac{\mathrm{d}p}{\mathrm{d}z} = \frac{F - A_2(z)}{A_1(z)}. \tag{27}$$

Since F is constant for all sections between the two coaxial tubes, the pressure drop across the length of the overlapping stenosis is given as

$$\Delta p = \int_0^L \left(-\frac{\mathrm{d}p}{\mathrm{d}z}\right)\mathrm{d}z. \tag{28}$$

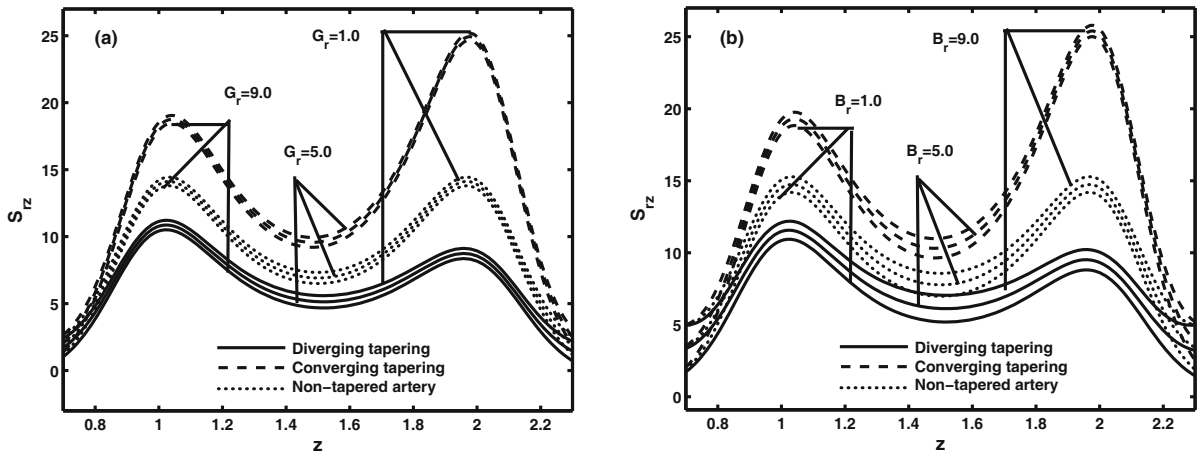

Fig. 2. Variation of the wall shear stress for (a) $B_r = 2.0$, for (b) $G_r = 2.0$; other parameters are $\delta = 0.1$, $N_t = 7.0$, $N_b = 0.5$, $\sigma = 0.75$, $F = 0.4$, $\alpha = 0.1$, $\omega = 7.854$, $R_c = 0.1$, $t = 0.5$.

Using the above eq. (28), the impedance resistance can be evaluated as

$$\lambda = \frac{\Delta p}{F} = \left\{ \int_0^{\sigma} K(z) \mid_{h=(mz+1)Q_1(t)} \mathrm{d}z + \int_{\sigma}^{\sigma+\frac{3}{2}} I(z)\mathrm{d}z + \int_{\sigma+\frac{3}{2}}^{L} K(z) \mid_{h=(mz+1)Q_1(t)} \mathrm{d}z \right\}, \tag{29}$$

where

$$I(z) = K(z) \mid_{h=(mz+1)Q_1(t)} . \tag{30}$$

The expression for the wall shear stress is given as [7]

$$S_{rz} = -\left(\frac{\partial w}{\partial r}\right)_{r=h}. \tag{31}$$

Using eq. (25) in the above eq. (31), we get

$$\begin{aligned} S_{rz} = -\frac{\mathrm{d}p}{\mathrm{d}z}\frac{1}{144h(\ln h - \ln R_c)}\Big(\Big(36(h^2(-1+2\ln h - 2\ln R_c)) + R_c^2\Big) + h^2 \\ \Big(-36a_1 + 27a_4 - h(16a_2 + 9a_3h) + 6\ln h(12a_1 - 9a_4 + 8a_2h + 6a_3 \\ h^2 + 12a_4\ln h\Big) - 6(12a_1 - 3a_4 + 8a_2h + 6a_3h^2 + 12a_4\ln h)\ln R_c\Big) \\ 9(4a_1 - 3a_4 + 4a_4\ln R_c)R_c^2 + 16a_2R_c^3 + 9a_3R_c^4. \end{aligned} \tag{32}$$

3 Graphical results and discussion

In order to understand the quantitative effects of thermophoresis number N_t, Brownian motion number N_b, local nanoparticle Grashof number G_r and local temperature Grashof number B_r,we have plot the graphs of wall shear stress, impedance resistance to flow, nanoparticle volume fraction, temperature distribution and axial velocity by considering three distinct arteries. In figs. 2 and 3 the variations of wall shear stress *versus* z are shown to understand the development of arterial disease with different flow parameters. We can see that wall shear stress gives higher results for convergent tapering as associated with other tapering arteries. The wall shear stress for different values of local nanoparticle Grashof number G_r and local temperature Grashof number B_r are given in figs. 2(a) and (b). In these figures we observed that the wall shear stress decreases with an increase in G_r, while it increases with an increase in B_r. The variation of the wall shear stress for different values of thermophoresis number N_t, Brownian motion number N_b *versus* axial distance z are given in figs. 3(a) and (b). It is illustrated from these graphs that the stress on the wall of arteries decreases with an increase in N_b, while it increases with an increase in N_t. Figures 4 and 5 depict the variation of the resistance impedance to the flow along the maximum height of stenosis δ for different values of the tapering angle φ.

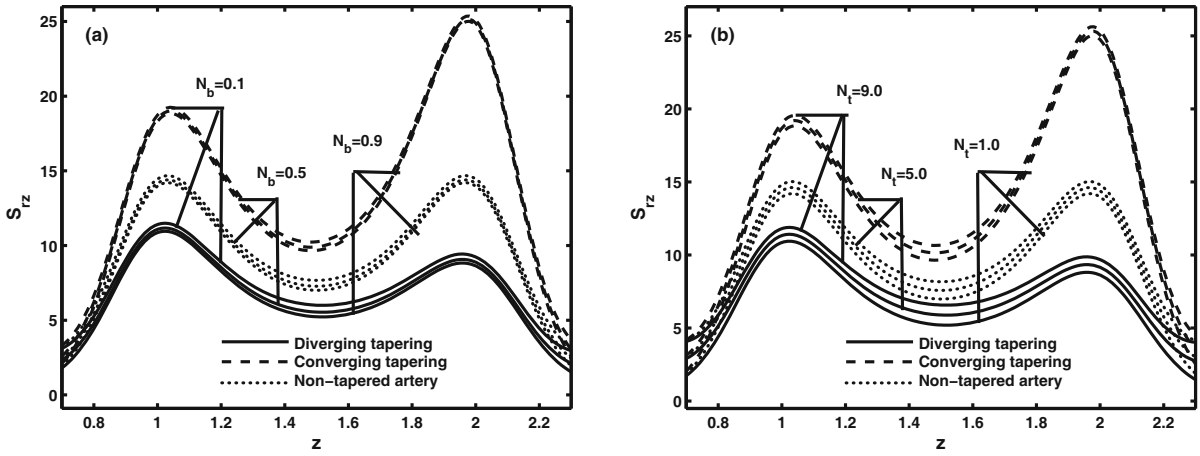

Fig. 3. Variation of the wall shear stress for (a) $N_t = 7.0$, for (b) $N_b = 0.5$; other parameters are $\delta = 0.1$, $B_r = 2.0$, $G_r = 2.0$, $\sigma = 0.75$, $F = 0.4$, $\alpha = 0.1$, $\omega = 7.854$, $R_c = 0.1$, $t = 0.5$.

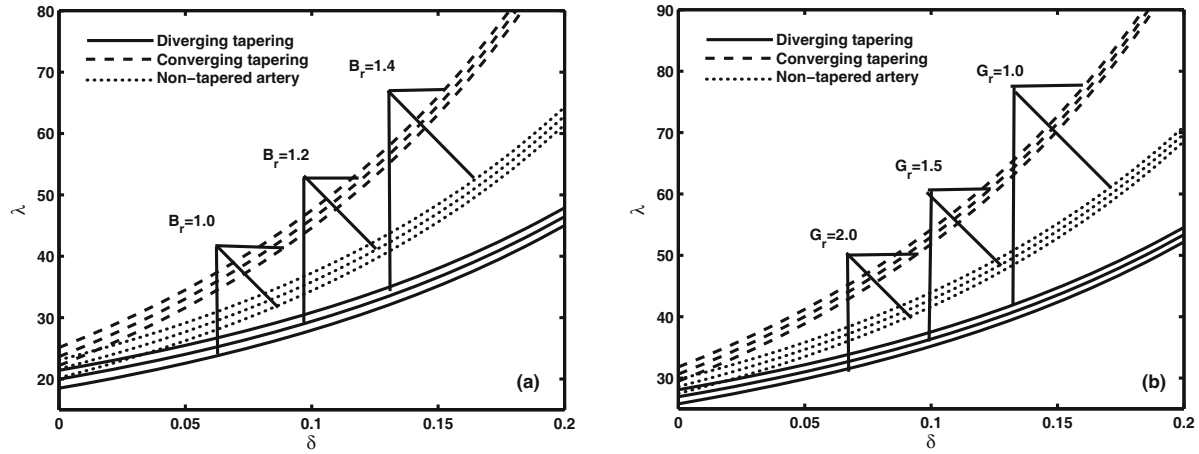

Fig. 4. Variation of the resistance impedance for (a) $G_r = 2.0$, (b) $B_r = 2.0$; other parameters are $\delta = 0.1$, $N_t = 5.0$, $N_b = 0.5$, $\sigma = 0.75$, $F = 0.4$, $\alpha = 0.1$, $\omega = 7.854$, $R_c = 0.1$, $t = 0.5$.

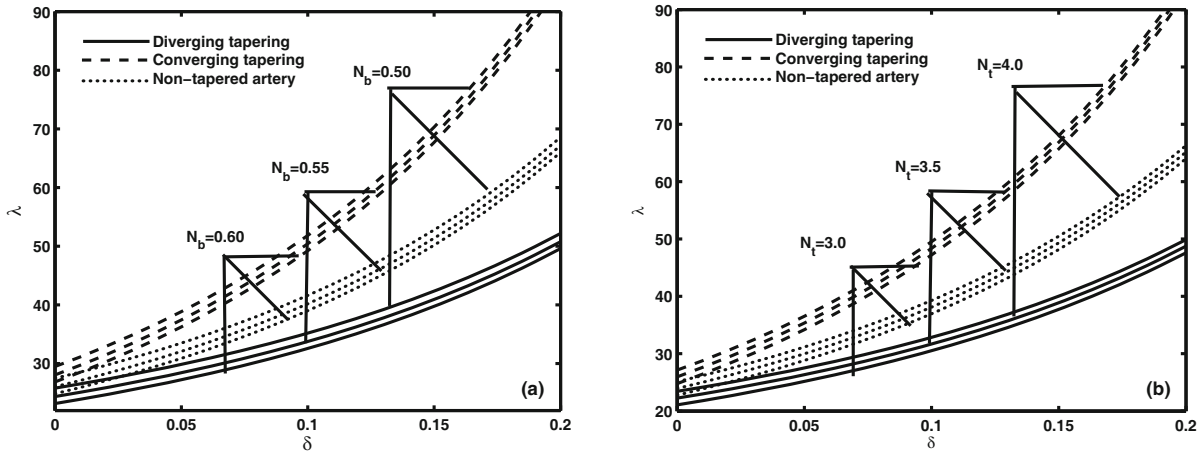

Fig. 5. Variation of the resistance impedance for (a) $N_t = 5.0$, for (b) $N_b = 0.5$; other parameters are $\delta = 0.1$, $G_r = 2.0$, $B_r = 2.0$, $\sigma = 0.75$, $F = 0.4$, $\alpha = 0.1$, $\omega = 7.854$, $R_c = 0.1$, $t = 0.5$.

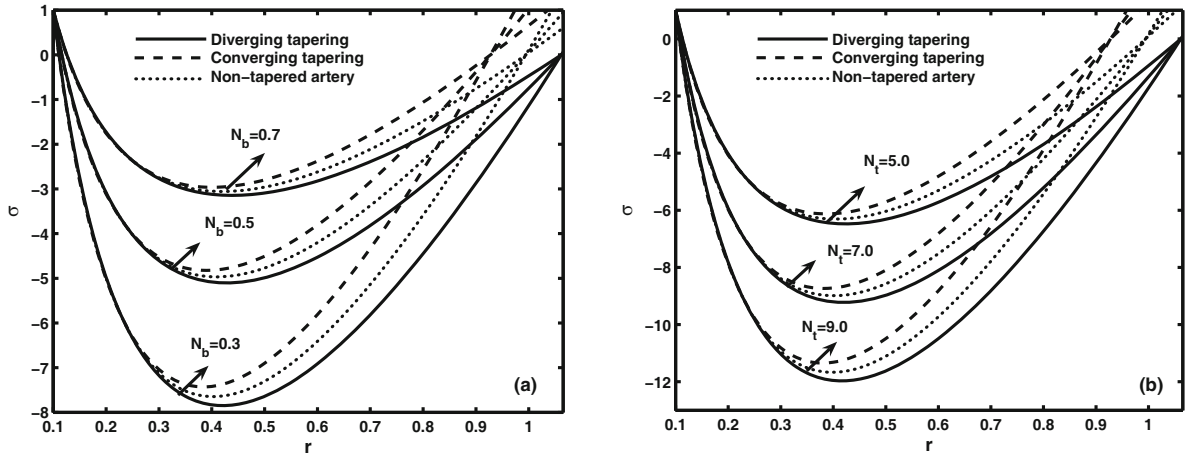

Fig. 6. Variation of the nanoparticle volume fraction for (a) $N_t = 7.0$, for (b) $N_b = 0.5$; other parameters are $\delta = 0.1$, $\sigma = 0.75$, $F = 0.4$, $\alpha = 0.1$, $\omega = 7.854$, $R_c = 0.1$, $t = 0.5$.

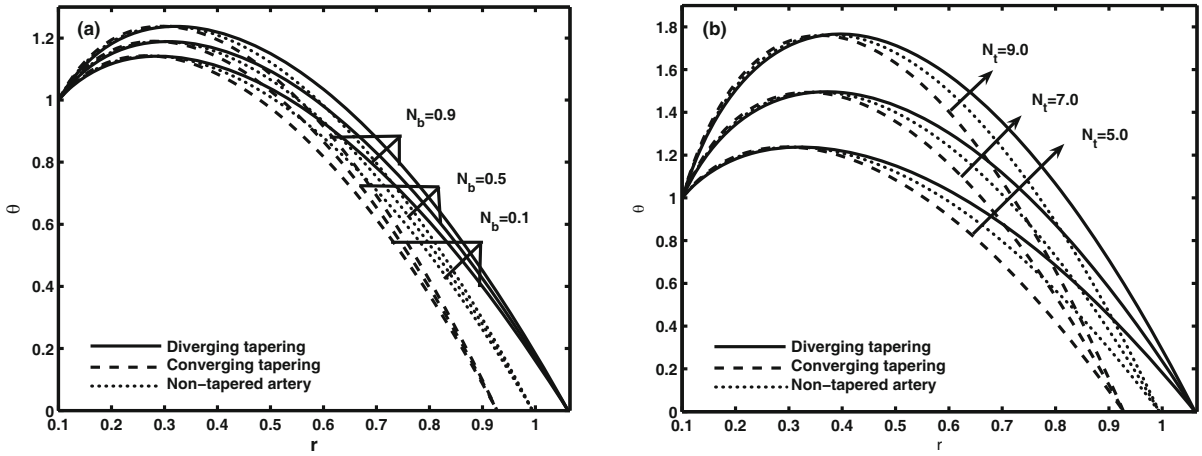

Fig. 7. Variation of the temperature distribution for (a) $N_t = 7.0$, for (b) $N_b = 0.5$; other parameters are $\delta = 0.1$, $\sigma = 0.75$, $F = 0.4$, $\alpha = 0.1$, $\omega = 7.854$, $R_c = 0.1$, $t = 0.5$.

It is analyzed that the resistance impedance to the flow gives larger values for converging tapering as comparing to other tapering arteries. The variations of the local nanoparticle Grashof number G_r and the local temperature Grashof number B_r are given in figs. 4(a) and (b). It is analyzed that resistance impedance to flow increases with an increase in B_r, while decreases with an increase in G_r. Figures 5(a) and (b) are plotted for different values of thermophoresis number N_t and Brownian motion number N_b. It is found from these graphs that the resistance impedance to the flow decreases with an increase in N_b, while it increases with an increase in N_t. The variations of the nanoparticle volume fraction for different values of thermophoresis number N_t and Brownian motion number N_b are shown in figs. 6(a) and (b). It is observed from these graphs that the nanoparticle volume fraction increases with an increase in N_b, while it decreases with an increase in N_t. The graphs of the nanoparticle volume fraction give larger values for divergent tapering between the interval $0.1 \leq r \leq 0.27$ and gives opposite results in the interval $0.28 \leq r \leq h$. The variations of the temperature distribution for different values of thermophoresis number N_t and Brownian motion number N_b are given in figs. 7(a) and (b). It is shown that the temperature distribution increases with an increase in the values of thermophoresis number N_t and Brownian motion number N_b. From these figures it is observed that temperature distribution gives higher results for convergent tapering between the interval $0.1 \leq r \leq 0.35$, while it gives higher results for divergent tapering between the interval $0.36 \leq r \leq h$. Figures 8 and 9 are plotted to observe the influence of the axial velocity w on the blood flow through overlapping stenosis. It is observed that the velocity profile between the interval $0.1 \leq r \leq 0.60$ ($\varphi \prec 0$), $0.1 \leq r \leq 0.69$ ($\varphi \succ 0$), $0.1 \leq r \leq 0.64$ ($\varphi = 0$) increases with an increase in the values of the local nanoparticle Grashof number G_r, Brownian motion number N_b and it decreases with an increase in the values of local temperature Grashof number B_r and thermophoresis number N_t, while an opposite trend is

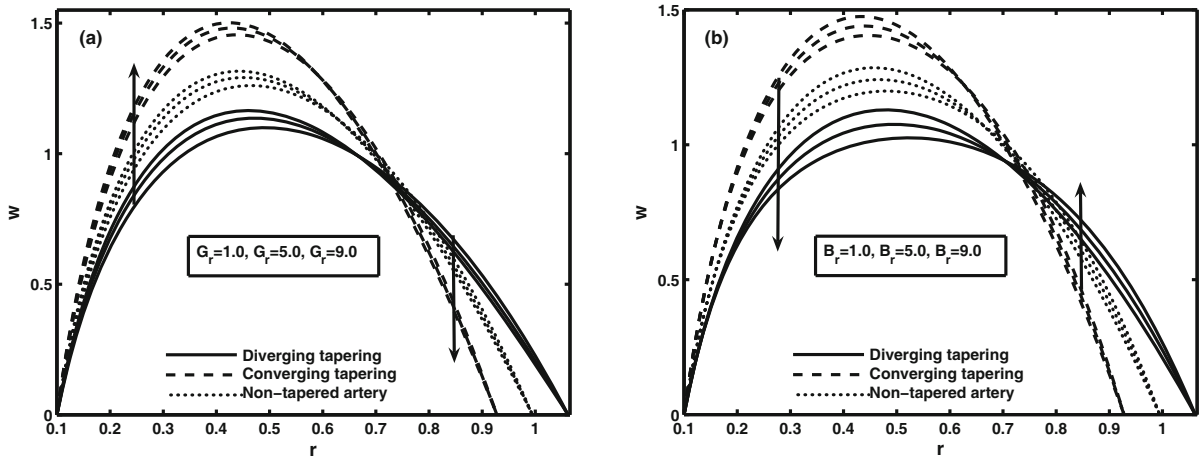

Fig. 8. Variation of the axial velocity for (a) $B_r = 2.0$, for (b) $G_r = 2.0$; other parameters are $\delta = 0.1$, $N_t = 7.0$, $N_b = 0.5$, $\sigma = 0.75$, $F = 0.4$, $\alpha = 0.1$, $\omega = 7.854$, $R_c = 0.1$, $t = 0.5$.

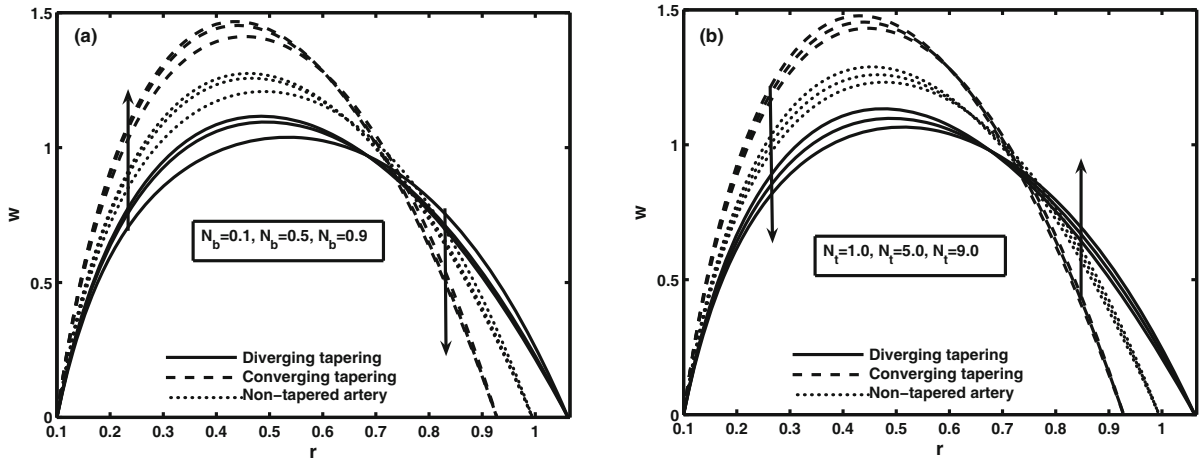

Fig. 9. Variation of the velocity profile for (a) $N_t = 7.0$, for (b) $N_b = 0.5$; other parameters are $\delta = 0.1$, $G_r = 2.0$, $B_r = 2.0$, $\sigma = 0.75$, $F = 0.4$, $\alpha = 0.1$, $\omega = 7.854$, $R_c = 0.1$, $t = 0.5$.

observed in the interval between $0.60 \leq r \leq h$ ($\varphi \prec 0$), $0.70 \leq r \leq h$ ($\varphi \succ 0$), $0.65 \leq r \leq h$ ($\varphi = 0$). It is also analyzed that the axial velocity gives higher results for convergent tapering. Figures 10 to 12 are plotted *versus* time t for almost four and three cardiac phases. In these graphs we can see that the magnitude of the first cycle starts increasing to obtain its maximum then starts decreasing to obtain its minimum then replicates its form again to obtain the starting point of the second cycle and so on. It is also observed that these graphs decay as the time t increases. The trapping phenomenon for the blood flow in an overlapping stenosed artery is discussed through figs. 13 to 19. From figs. 13 to 19, it is observed that size of the trapping bolus decreases with an increase in the local nanoparticle Grashof number G_r, thermophoresis number N_t, Brownian motion number N_b and catheter size R_c, while it increases with an increase in time t and local temperature Grashof number B_r. It is also observed that the trapping bolus moves towards point $z = 1.5$. It is observed that the trapping bolus for φ decreases in the right-hand side of the z-axis for divergent tapering, while it decreases in the left-hand side of the z-axis for convergent tapering. Tables 1, 2 and 3 are plotted for velocity profile, nanoparticle volume fraction and temperature distribution with different variations of stenosis height. It is observed, from table 1, that the axial velocity increases between the interval $0.1 \leq r \leq 0.7$ and gives larger values for convergent tapering, while it decreases between the interval $0.8 \leq r \leq h$ and gives larger values for divergent tapering. From tables 2 and 3, it is observed that the temperature distribution increases between the interval $0.1 \leq r \leq 0.3$, while it decreases between the interval $0.31 \leq r \leq h$ and nanoparticle volume fraction decreases in the whole domain of r with an increase in the stenosis height δ.

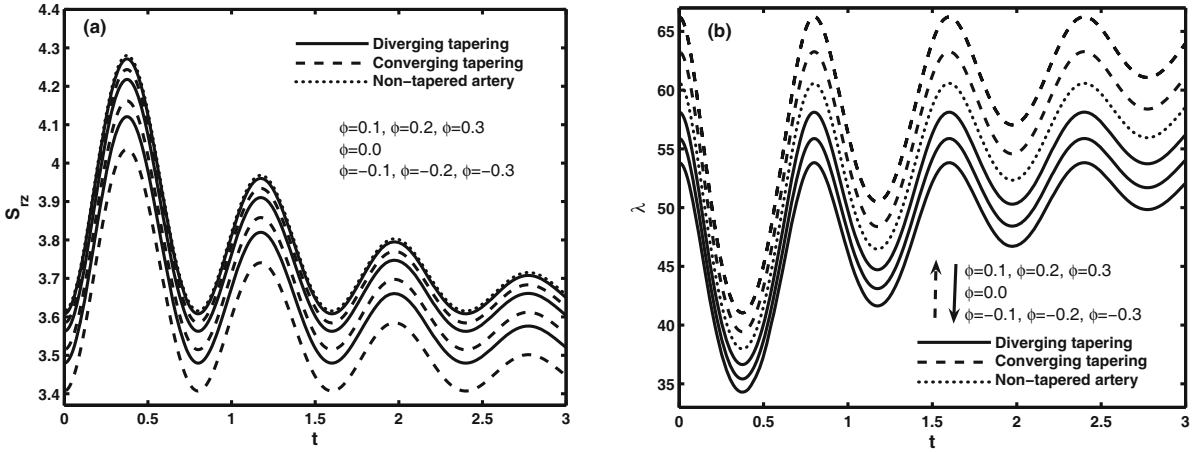

Fig. 10. Variation of the wall shear stress and resistance impedance with t for $\delta = 0.1$, $G_r = 2.0$, $B_r = 2.0$, $\sigma = 0.75$, $F = 0.4$, $\alpha = 0.1$, $\omega = 7.854$, $N_t = 7.0$, $N_b = 0.5$, $R_c = 0.1$.

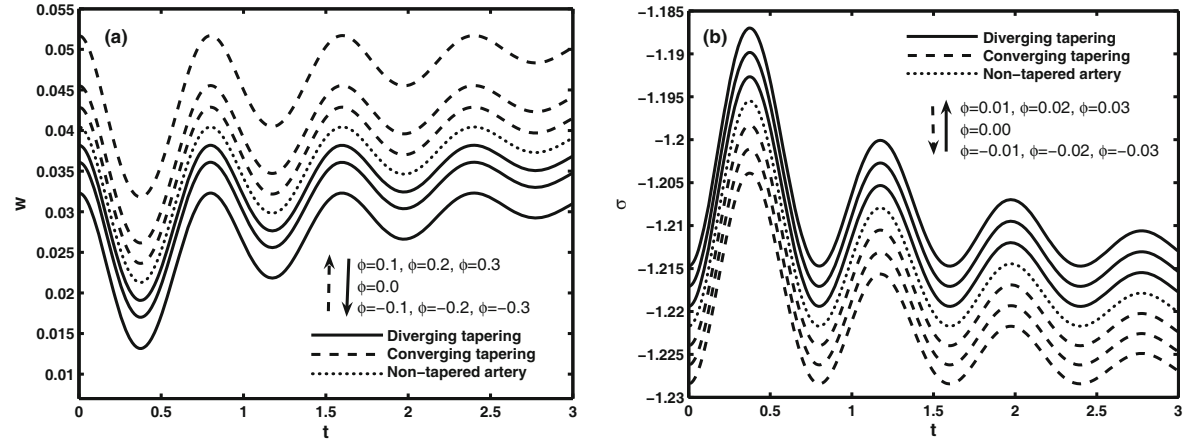

Fig. 11. Variation of the axial velocity profile and nanoparticle concentration with t for $\delta = 0.1$, $G_r = 2.0$, $B_r = 2.0$, $\sigma = 0.75$, $F = 0.4$, $\alpha = 0.1$, $\omega = 7.854$, $N_t = 7.0$, $N_b = 0.5$, $R_c = 0.1$.

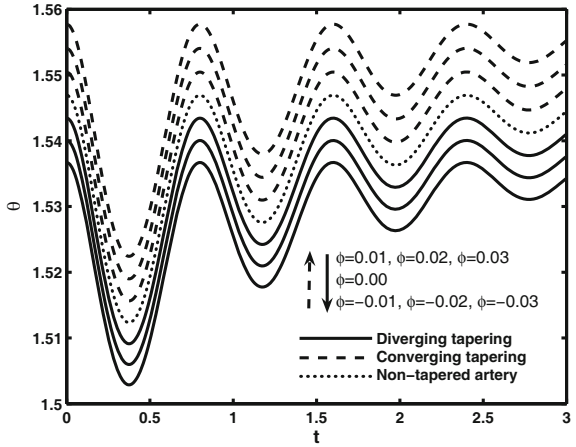

Fig. 12. Variation of the temperature profile with t for $\delta = 0.1$, $G_r = 2.0$, $B_r = 2.0$, $\sigma = 0.75$, $F = 0.4$, $\alpha = 0.1$, $\omega = 7.854$, $N_t = 7.0$, $N_b = 0.5$, $R_c = 0.1$.

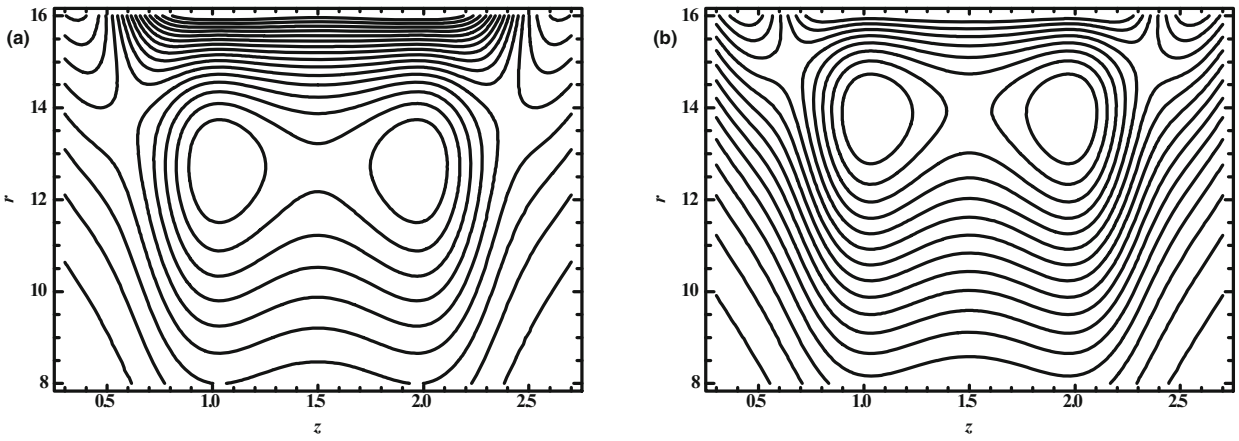

Fig. 13. Blood flow pattern for (a) $B_r = 0.4$, (b) $B_r = 0.45$; other parameters are $\delta = 0.1$, $N_t = 0.7$, $N_b = 0.06$, $\sigma = 0.75$, $F = 0.32$, $\alpha = 0.1$, $\omega = 7.854$, $G_r = 3.0$, $R_c = 0.1$, $t = 0.5$.

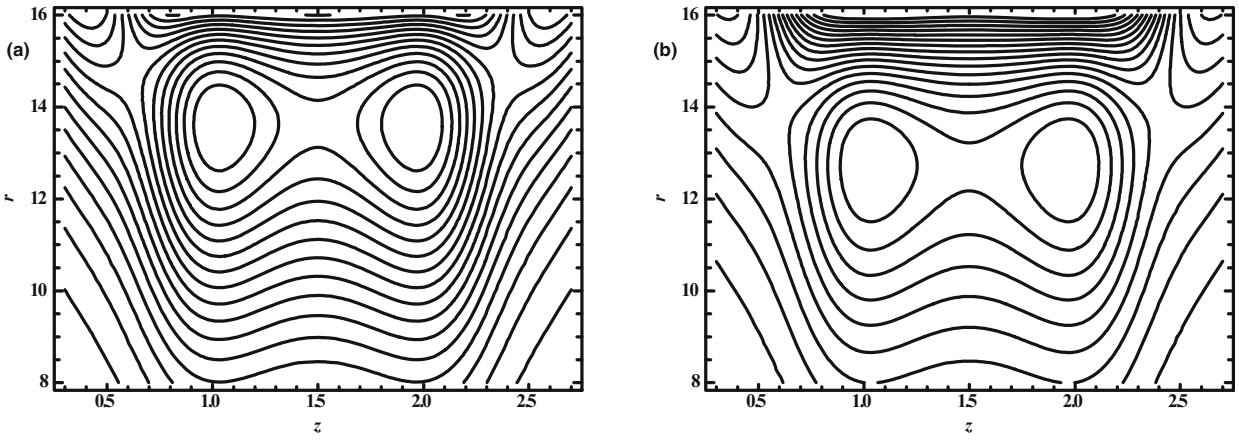

Fig. 14. Blood flow pattern for (a) $G_r = 2.9$, (b) $G_r = 3.2$; other parameters are $\delta = 0.1$, $N_t = 0.7$, $N_b = 0.06$, $\sigma = 0.75$, $F = 0.32$, $\alpha = 0.1$, $\omega = 7.854$, $B_r = 0.4$, $R_c = 0.1$, $t = 0.5$.

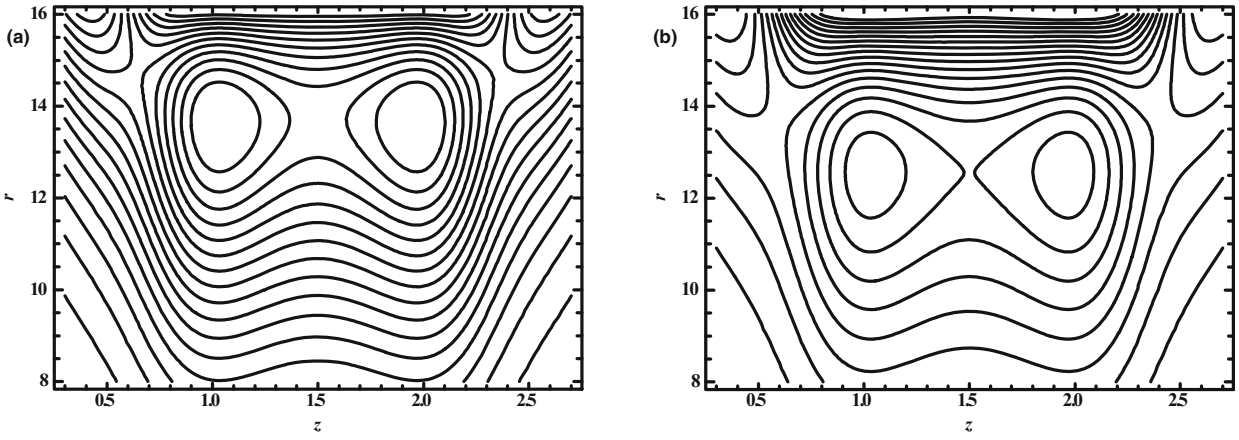

Fig. 15. Blood flow pattern for (a) $N_b = 0.055$, (b) $N_b = 0.06$; other parameters are $\delta = 0.1$, $N_t = 0.7$, $\sigma = 0.75$, $F = 0.32$, $\alpha = 0.1$, $\omega = 7.854$, $B_r = 0.4$, $t = 0.5$, $R_c = 0.1$, $G_r = 3.2$.

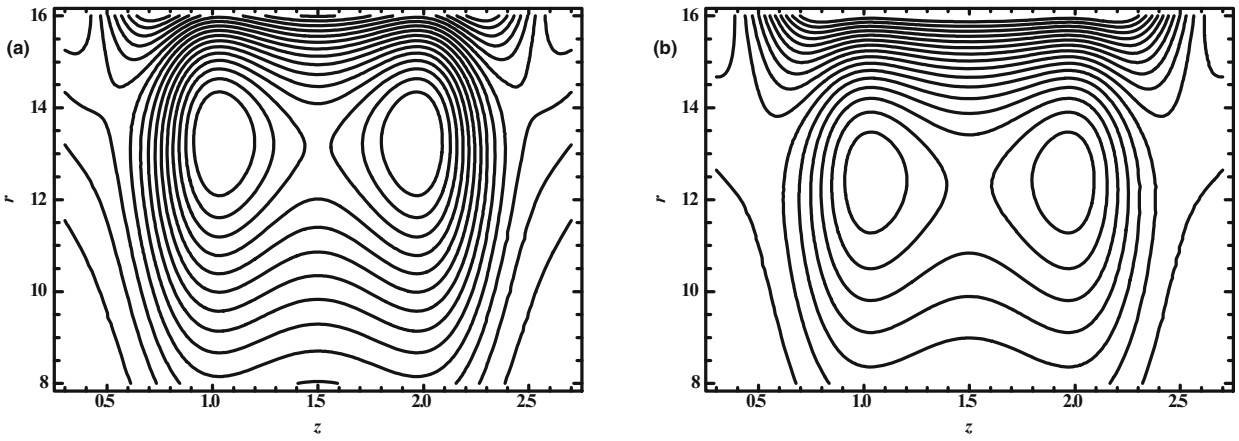

Fig. 16. Blood flow pattern for (a) $N_t = 0.5$, (b) $N_t = 0.8$; other parameters are $\delta = 0.1$, $N_b = 0.06$, $\sigma = 0.75$, $F = 0.32$, $\alpha = 0.1$, $\omega = 7.854$, $B_r = 0.4$, $t = 0.5$, $R_c = 0.1$, $G_r = 3.2$.

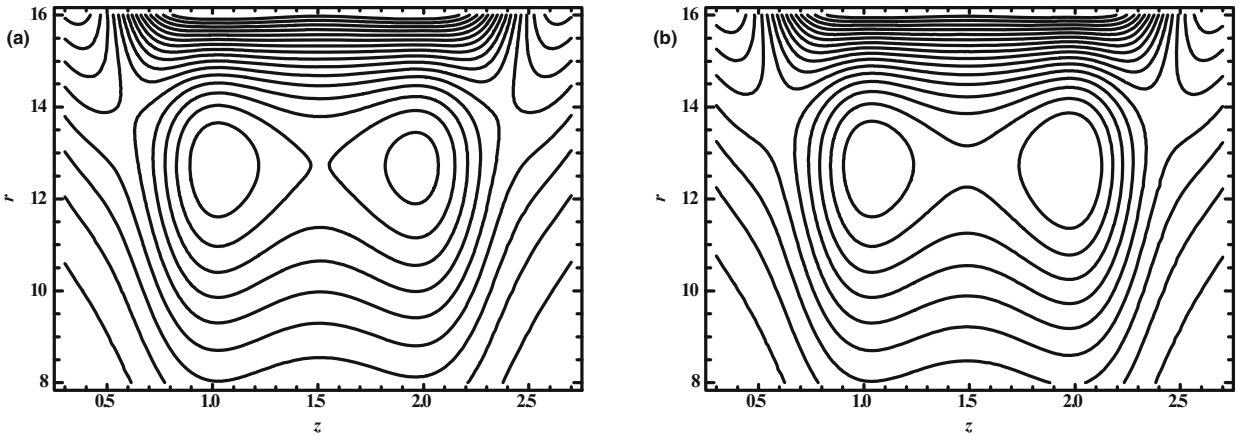

Fig. 17. Blood flow pattern for (a) $\varphi = 0.01$, (b) $-\varphi = 0.01$; other parameters are $\delta = 0.1$, $N_b = 0.06$, $\sigma = 0.75$, $F = 0.32$, $\alpha = 0.1$, $\omega = 7.854$, $B_r = 0.4$, $t = 0.5$, $N_t = 0.5$, $R_c = 0.1$, $G_r = 3.2$.

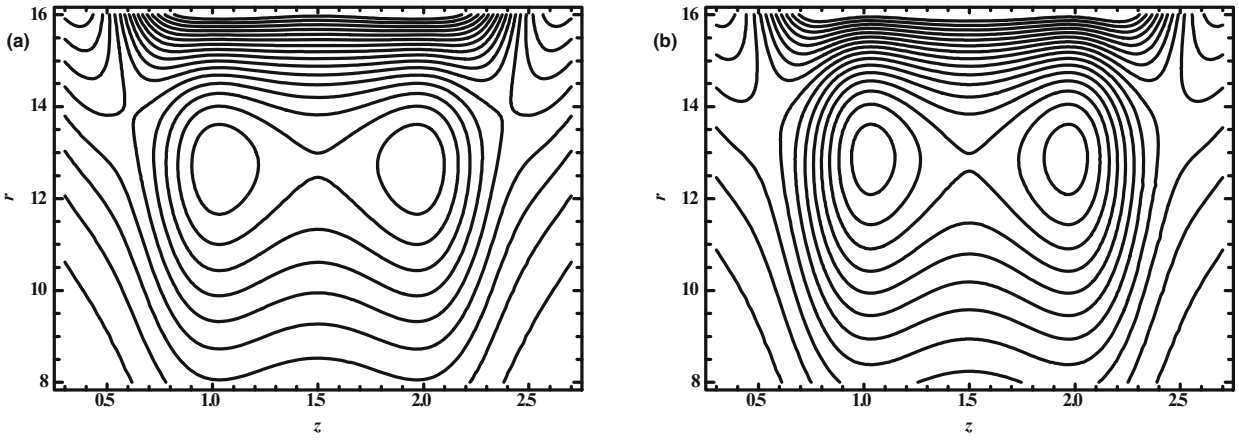

Fig. 18. Blood flow pattern for (a) $t = 0.3$, (b) $t = 0.6$; other parameters are $\delta = 0.1$, $N_b = 0.06$, $\sigma = 0.75$, $F = 0.32$, $\alpha = 0.1$, $\omega = 7.854$, $B_r = 0.4$, $N_t = 0.5$, $R_c = 0.1$, $G_r = 3.2$.

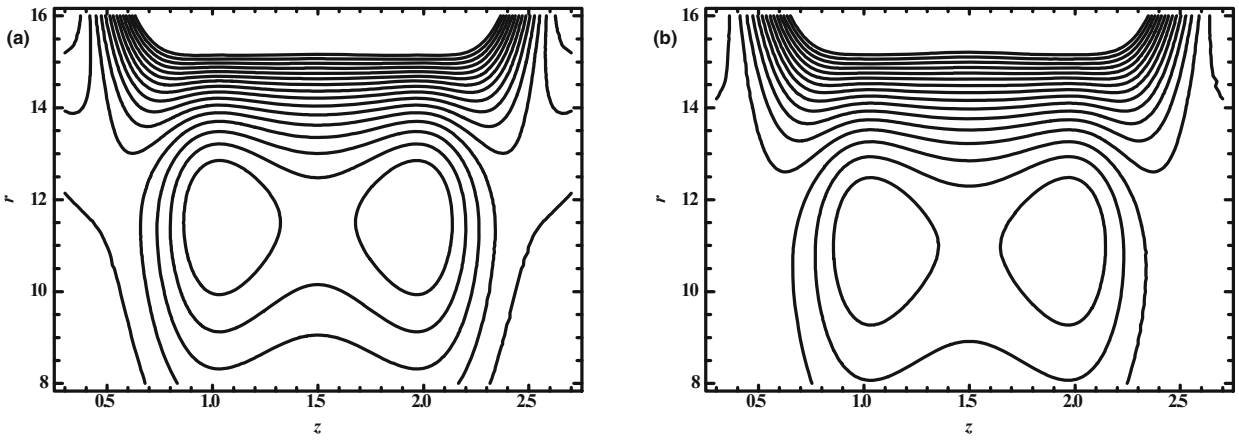

Fig. 19. Blood flow pattern for (a) $R_c = 0.2$, (b) $R_c = 0.3$; other parameters are $\delta = 0.1$, $N_b = 0.06$, $\sigma = 0.75$, $F = 0.32$, $\alpha = 0.1$, $\omega = 7.854$, $B_r = 0.4$, $N_t = 0.5$, $G_r = 3.2$, $t = 0.3$.

Table 1. Variation for the axial velocity.

φ	Diverging tapering $\succ$		Converging tapering $\prec$		Non-tapered artery	
r	$\delta = 0.07$	$\delta = 0.1$	$\delta = 0.07$	$\delta = 0.1$	$\delta = 0.07$	$\delta = 0.1$
0.1	0.0000000	0.0000000	0.0000000	0.0000000	0.0000000	0.0000000
0.2	0.6012620	0.6531000	0.8299610	0.9132460	0.7025470	0.7678200
0.3	0.8778750	0.9510750	1.1965600	1.3100000	1.0203600	1.1110400
0.4	1.0065300	1.0852400	1.3419900	1.4569000	1.1588200	1.2537900
0.5	1.0419000	1.1147200	1.3409600	1.4361800	1.1813700	1.2652700
0.6	1.0068600	1.0642800	1.2248700	1.2824800	1.1145900	1.1745000
0.7	0.9119760	0.9454540	1.0086400	1.0123600	0.9709270	0.9951840
0.8	0.7620900	0.7635760	0.6995110	0.6340320	0.7562470	0.7338730
0.9	0.5589840	0.5207490	0.3007410	0.1513460	0.4729530	0.3934060
h	0.0000000	0.0000000	0.0000000	0.0000000	0.0000000	0.0000000

Table 2. Variation for the nanoparticle volume fraction.

φ	Diverging tapering $\succ$		Converging tapering $\prec$		Non-tapered artery	
r	$\delta = 0.07$	$\delta = 0.1$	$\delta = 0.07$	$\delta = 0.1$	$\delta = 0.07$	$\delta = 0.1$
0.1	1.0000000	1.0000000	1.0000000	1.0000000	1.0000000	1.0000000
0.2	1.1785100	1.1815300	1.1904900	1.1941300	1.1842300	1.1875500
0.3	1.2348500	1.2359500	1.2377700	1.2378100	1.2367400	1.2374300
0.4	1.2236800	1.2194900	1.2030700	1.1944400	1.2152000	1.2091600
0.5	1.1621100	1.1497500	1.1055800	1.0839200	1.1376900	1.1214100
0.6	1.0577700	1.0346100	0.9538340	0.9150870	1.0122700	0.9824750
0.7	0.9147390	0.8782250	0.7524050	0.6926670	0.8432210	0.7967940
0.8	0.7354430	0.6831150	0.5040090	0.4194800	0.6331140	0.5670130
0.9	0.5214490	0.4508850	0.2104030	0.0973437	0.3836020	0.2948390
h	0.0000000	0.0000000	0.0000000	0.0000000	0.0000000	0.0000000

Table 3. Variation for the temperature distribution.

φ	Diverging tapering $\succ$		Converging tapering $\prec$		Non-tapered artery	
r	$\delta = 0.07$	$\delta = 0.1$	$\delta = 0.07$	$\delta = 0.1$	$\delta = 0.07$	$\delta = 0.1$
0.1	1.0000000	1.0000000	1.0000000	1.0000000	1.0000000	1.0000000
0.2	−4.016470	−4.028920	−4.059960	−4.070080	−4.039190	−4.050740
0.3	−5.910990	−5.891550	−5.818660	−5.782140	−5.872040	−5.845160
0.4	−6.527310	−6.457840	−6.225760	−6.119360	−6.392150	−6.306370
0.5	−6.443250	−6.313810	−5.892250	−5.703250	−6.192950	−6.037050
0.6	−5.916190	−5.720480	−5.090290	−4.810630	−5.538770	−5.305670
0.7	−5.083410	−4.817100	−3.965060	−3.589190	−4.570620	−4.255410
0.8	−4.026870	−3.686780	−2.603220	−2.127060	−3.372650	−2.971770
0.9	−2.799430	−2.383130	−1.060660	−0.481109	−1.999170	−1.509860
h	0.0000000	0.0000000	0.0000000	0.0000000	0.0000000	0.0000000

4 Conclusion

The influence of the catheter on the blood flow through a tapered artery with overlapping stenosis is considered in this paper. The graphical results are obtained for the axial velocity, nanoparticle volume fraction, temperature distribution, wall shear stress distributions, resistance impedance to the flow and streamlines. The main results of the present study can be listed as follows:

- The wall shear stress and resistance impedance to the flow give higher results for the converging tapering as compared to diverging tapering and non-tapered arteries.
- The wall shear stress and resistance impedance possess the same behavior for thermophoresis number N_t, local nanoparticle Grashof number G_r, local temperature Grashof number B_r and Brownian motion number N_b parameters.
- The nanoparticle volume fraction increases with an increase in the Brownian motion number N_b and decreases with an increases in the thermophoresis number N_t.
- The temperature distribution increases with an increase in the Brownian motion number N_b and thermophoresis number N_t.
- The axial velocity gives higher results for convergent tapering and shows opposite results for Brownian motion number N_b and thermophoresis number N_t.
- The variations of graphs *versus* t for almost four and three cardiac phases shows that oscillations decay as the time t increases.
- The number of trapping bolus decreases with an increase in cather size R_c.

Appendix A.

$$a_1 = \Big(4B_rN_t(h-R_c)(h\ln R_c - R_c\ln h) + G_rN_b^2(-h^2\ln R_c + R_c^2\ln h)N_b\Big(4(B_r+G_r)$$

$$\ln h(h-R_c)^2 + G_rN_t(-h^2\ln R_c + R_c^2\ln h)\Big)\Big)/4(\ln h - \ln R_c)N_b(h-R_c)^2,$$

$$a_2 = B_rN_t/N_b(h-R_c),\ a_3 = -G_r(N_t+N_b)/4(h-R_c)^2,$$

$$a_4 = 4B_rN_t(-h+R_c) + G_rN_b^2(h+R_c) + N_b\Big(-4(B_r+G_r)(h-R_c) + G_rN_t(h+R_c)\Big)/$$

$$4(\ln h - \ln R_c)N_b(h-R_c),$$

$$A_1 = -720(\ln h - \ln R_c)N_b(h-R_c)^2(h+R_c)\Big(h^2(-1+\ln h - \ln R_c) + (1+\ln h$$

$$-\ln R_c)\Big)R_c^2/11520(\ln h - \ln R_c)^2N_b(h-R_c),$$

$$
\begin{aligned}
A_2 = {} & 15G_rN_b^2(h+R_c)(h^4(9+8(\ln h)^2+\ln R_c(15+8\ln R_c)-\ln h(15+16\ln R_c)) \\
& +2h^2(-9+4(\ln h-\ln R_c)^2R_c^2+(9+15\ln h+8(\ln h)^2-(15+16\ln h)\ln R_c \\
& +8(\ln R_c)^2)R_c^4)-4B_rN_t(h^5135+84(\ln h)^2+2\ln R_c(95+42\ln R_c)-2\ln h(95 \\
& +84\ln R_c))45h^4(-3+2\ln h-2\ln R_c)R_c+10h^3(-27+10\ln h-10\ln R_c)R_c^2 \\
& +10h^2(27+10\ln h-10\ln R_c)R_c^3+45h(3+2\ln h-2\ln R_c)R_c^4-(135+190 \\
& \ln h+84(\ln h)^2-2(95+84\ln h)\ln R_c+84(\ln R_c)^2)R_c^5)+15N_b(12(B_r+G_r) \\
& (h-R_c)(h^4(-3+2\ln h-2\ln R_c)+2h^2(3+2\ln h-2\ln R_c)R_c^2-(3+6\ln h \\
& +4(\ln h)^2-2(3+4\ln h)\ln R_c+4(\ln R_c)^2)R_c^4)+G_rN_t(h+R_c)\ (h^4(9+8(\ln h)^2 \\
& +\ln R_c(15+8\ln R_c)-\ln h(15+16\ln R_c))+2h^2(-9+4(\ln h-\ln R_c)^2)R_c^2(9 \\
& +15\ln h+8(\ln h)^2-(15+16\ln h)\ln R_c+8(\ln R_c)^2)\ R_c^4))/11520(\ln h-\ln R_c)^2 \\
& N_b(h-R_c).
\end{aligned}
$$

References

1. F.D. Young, F.Y. Tsai, J. Biomech. **6**, 395 (1973).
2. B. Liu, D. Tang, Appl. Numer. Math. **32**, 87 (2000).
3. M. Texon, Arch. Int. Med. **99**, 418 (1957).
4. G.T. Liu, X.J. Wang, B.Q. Ai, L.G. Liu, Chin. J. Phys. **42**, 401 (2004).
5. M. Massoudi, T.X. Phuoc, Comput. Math. Appl. **56**, 199 (2008).
6. S. Nadeem, N.S. Akbar, Taiwan J. Math. **42**, 67 (2011).
7. Kh.S. Mekheimer, M.H. Haroun, M.A. El Kot, Can. J. Phys. **89**, 201 (2011).
8. S. Chakravarty, P.K. Mandal, Math. Comput. Model. **24**, 43 (1996).
9. Kh.S. Mekheimer, M.H. Haroun, M.A. El Kot, Appl. Math. Inf. Sci. **2**, 281 (2012).
10. Z. Ismail, I. Abdullah, N. Mustapha, N. Amin, Appl. Math. Comput. **95**, 669 (2008).
11. Kh.S. Mekheimer, M.A. El Kot, Appl. Math. Model. **36**, 5393 (2012).
12. G.C. Layek, S. Mukhopadhyay, R.S.R. Gorla, Int. J. Eng. Sci. **47**, 649 (2009).
13. S. Chakravarty, P.K. Mandal, Int. J. Non-Linear Mech. **35**, 779 (2000).
14. Kh.S. Mekheimer, M.A. El Kot, Chem. Eng. Comm. **197**, 1195 (2010).
15. V.P. Srivastava, R. Rastogi, Comput. Math. Appl. **59**, 1377 (2010).
16. Kh.S. Mekheimer, M.A. El Kot, Int. J. Non-linear Mech. **47**, 927 (2012).
17. V.P. Srivastava, R. Srivastava, Comput. Math. Appl. **58**, 227 (2009).
18. N.K. Vermaa, S. Mishrab, S.U. Siddiqui, R.S. Gupta, Adv. Appl. Sci. Res. **2**, 114 (2011).
19. S.U.S. Choi, ASME **36**, 99 (1995).
20. J. Buongiorno, J. Heat Transfer **128**, 240 (2005).
21. S. Noreen, Eur. Phys. J. Plus **129**, 33 (2014).
22. F. Gentile, M. Ferrari, P. Decuzzi, Ann. Biomed. Eng. **36**, 254 (2007).
23. N.S. Akbar, IEEE Trans. Nanotechnol. **13**, 357 (2014).
24. N.S. Akbar, M. Raza, R. Ellahi, Eur. Phys. J. Plus **129**, 155 (2014).
25. S. Nadeem, S. Ijaz, N.S. Akbar, J. Comput. Theor. Nanosci. **10**, 2751 (2013).
26. S. Nadeem, S. Ijaz, N.S. Akbar, Int. Nano Lett. **3**, 35 (2013).
27. N.S. Akbar, S.U. Rahman, R. Ellahi, S. Nadeem, Int. J. Therm. Sci. **85**, 54 (2014).
28. R. Ellahi, S.U. Rahman, S. Nadeem, Phys. Lett. A **378**, 2973 (2014).
29. S. Nadeem, S. Ijaz, M.A. Sadiq, Curr. Nanosci. **13**, 753 (2014).
30. J.H. He, Chaos Solitons Fractals **26**, 695 (2005).
31. J.H. He, Comput. Methods. Appl. **135**, 73 (2003).